Poisoning effects of KCl and As$_2$O$_3$ on selective catalytic reduction of NO with NH$_3$ over Mn-Ce/AC catalysts at low temperature

Shan Ren[a,*], Shulan Li[a], Zenghui Su[a], Jie Yang[a], Hongming Long[b], Ming Kong[a], Jian Yang[a], Zelong Cai[a]

[a] College of Materials Science and Engineering, Chongqing University, Chongqing 400044, China
[b] School of Metallurgical Engineering, Anhui University of Technology, Ma'anshan 243032, China

HIGHLIGHTS

- Effect of KCl and As$_2$O$_3$ on SCR denitration of Mn-Ce/AC catalyst was studied.
- Mn-Ce/AC catalyst deactivated seriously with the increase of KCl doping amount.
- As$_2$O$_3$ was oxidized to As$_2$O$_5$ to form coverage and reduce catalyst surface acidity.
- Synergy poisoning model of KCl and As$_2$O$_3$ on Mn-Ce/AC catalyst was proposed.

GRAPHICAL ABSTRACT
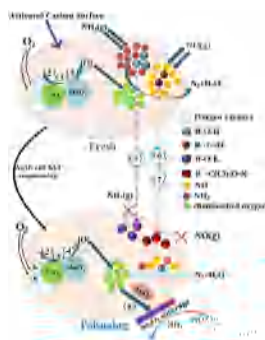
ABSTRACT

The poisoning effects of KCl and As$_2$O$_3$ on selective catalytic reduction (SCR) of NH$_3$ with NO over Mn-Ce/AC catalysts were investigated with the reaction temperature range of 100–250 °C. KCl and As$_2$O$_3$ poisoned catalysts were synthesized by impregnation method and catalytic activity test was performed under the condition of simulated flue gas. The changes of crystal structure, microstructure, surface atomic state, surface acidity and functional groups were characterized by XRD, SEM, BET, XPS, NH$_3$-TPD and FT-IR. Deactivation for single KCl or As$_2$O$_3$ doping catalyst was observed and severe synergistic inactivation occurred with the common effect of KCl and As$_2$O$_3$ on the catalyst. KCl destroyed the porosity of active carbon (AC) and could react with −OH and C=O on the surface of AC to ultimately form -O-K and Cl-C-O-K, resulting in the decrease of NH$_3$ and NO adsorption. Besides, KCl caused the reduction of oxygen vacancies and chemisorbed oxygen on the Mn-Ce/AC catalyst. Lattice oxygen of MnO$_x$ may be transformed to surface chemisorbed oxygen to oxidize As$_2$O$_3$. As$_2$O$_3$ was oxidized to As$_2$O$_5$ and some layer was formed on the surface of catalyst preventing NH$_3$ and NO adsorption. In addition, As$_2$O$_3$ could increase the number of oxygen vacancies and decrease the surface acidity of Mn-Ce/AC catalyst. According to the experimental results and theoretical analysis, the synergy poisoning model of KCl and As$_2$O$_3$ on Mn-Ce/AC catalysts was schematically established.

1. Introduction

Nitrogen oxide (NO_x) is a major industrial pollutant due to the burning of fossil fuels which has caused a lot of problems such as acid rain and photochemical smog [1,2]. Controlling the emission of NO_x has been widely studied and selective catalytic reduction of NO with NH_3 (NH_3-SCR) has been demonstrated as one of the most effective technology for the removal of NO_x in flue gas. The traditional commercial V_2O_5-WO_3/TiO_2 catalysts made a great success in SCR de-NO_x of the coal-fired power plants flue gas. However, it exposed a lot of negative sides, such as the high operation temperature (300–400 °C) and the toxicity of vanadium species [3–5]. Therefore, it was imperative to develop an environmental friendly and efficient SCR catalyst for low-temperature flue gas denitrification, such as sintering flue gas in iron and steel industry. Mn-based catalysts showed excellent activity at low temperature below 160 °C and a more extensive operating temperature window [6,7]. Ce-based catalysts greatly improved NH_3-SCR performance of NO, showing remarkable SO_2 tolerance and N_2 selectivity due to its large oxygen storage capacity and unique redox couple Ce^{3+}/Ce^{4+} [8,9]. It was reported that Mn-Ce mixed-oxide catalysts supported on carbon materials exhibited excellent low-temperature de-NO_x activities [10,11]. Activated carbon (AC) has been extensively reported to exhibit high surface areas and high pore volumes due to its porous nature. The excellent pore structure was thought to be beneficial for the uniform dispersion of active component on the catalyst [12]. After treating with nitric acid, there were various oxygen groups containing the CO_2-type and CO-type groups on the surface of AC [13], which were commonly considered to improve the adsorption of NH_3 and NO [14]. Additionally, carbon-based catalysts exhibited high denitrification rate and great resistance to SO_2 poisoning in the temperature range of 375–523 K [15]. Therefore, Mn-Ce/AC catalyst is a promising candidate for denitrification at low temperature for sintering flue gas.

The flue gas from sintering plants always contains alkali metals and heavy metals, such as K, Na, As_2O_3 etc. It is well known that these elements have serious effects on SCR catalyst and Mn-Ce/AC catalyst will face the challenge of poisoning when used to remove NO_x from the flue gas. The poisoning mechanism of Alkali metal derived from coal-fired power plants on SCR titanium-based catalysts has been wildly studied. Alkali metal generates physical adsorption, reduces the surface chemisorbed oxygen and causes the decline of Brønsted acid sites for Mn-Ce/TiO_2 catalyst, which causes deactivation of the Mn-Ce/TiO_2 catalysts in the temperature range of 150–300 °C [16]. As_2O_3 could be oxidized to As_2O_5 by surface chemisorption oxygen for commercial V_2O_5-WO_3/TiO_2 in the range of 200 to 500 °C [17], decreasing Ce^{3+} concentration and NO_x adsorption [18]. However, these poisoning effects of KCl and As_2O_3 are focused on titanium-based catalysts. There are few reports about effects of KCl and As_2O_3 over Mn-Ce/AC catalysts at lower temperature, let alone synergistic effects. Therefore, it is necessary to understand the effect of KCl and As_2O_3 on the performance of Mn-Ce/AC catalysts at low temperature.

In this study, single and combined effects of KCl and As_2O_3 over Mn-Ce/AC catalysts have been investigated. The effect of KCl and As_2O_3 on Mn-Ce/AC denitrification catalyst activity was studied from 100 °C to 250 °C. The prepared samples were widely detected by characterization of XRD, SEM, BET, XPS, NH_3-TPD and FT-IR. This work is aiming to explore the substantial changes in Mn-Ce/AC catalysts caused by KCl and As_2O_3 and reveal the mechanism of their synergistic effect.

2. Experimental

2.1. Pretreatment of activated carbon

The original coal-based activated carbon was purchased from Shanghai Xinhui Activated Carbon Co. Ltd. It was ground and sieved to 10–20 mesh and oxidized by 60% HNO_3 at 80 °C for 4 h, followed by washing with de-ionized water and drying at 110 °C for 6 h.

2.2. Catalyst preparation

The Mn-Ce/AC catalyst with MnO_2 (5.0 wt%) and CeO_2 (10.0 wt%) loadings was prepared by impregnation method with $Mn(NO)_3$ and $Ce(NO_3)_2 \cdot 6H_2O$ as the precursors, respectively. During impregnation, the mixture was exposed to an ultrasonic bath for 1 h and then heated at 60 °C with stirring until the liquid was totally eliminated. After treatment, the samples were dried at 110 °C for 6 h, followed by calcination at 400 °C for 4 h in N_2 atmosphere.

The KCl poisoned samples were prepared by impregnating the KCl aqueous solution onto the obtained Mn-Ce/AC catalyst. The received samples were labeled as Kx-Mn-Ce/AC catalyst, where x(x = 0.5, 1.0, 2.0) was the mass percentage of KCl in solution. The KCl solution loaded catalysts were then ultrasonically treated for 1 h, stirred at 60 °C for 4 h, dried at 110 °C for 6 h and calcined at 400 °C for 4 h in N_2 successively.

To obtain As_2O_3 poisoned samples, a portion of Mn-Ce/AC catalyst was immerged into As_2O_3 solutions with 2.0% mass concentration and then treated with the same procedure of preparing Kx-Mn-Ce/AC catalyst. The obtained sample was denoted as As-Mn-Ce/AC catalyst. K2.0-As-Mn-Ce/AC represented the KCl and As_2O_3 co-poisoned catalyst containing 2.0% KCl and 2.0% As_2O_3. The prepare process was similar to the process of KCl or As_2O_3 poisoned catalyst. The content (wt%) of K and As in the poisoned catalysts was detected by ICP-OES (PerkinElmer Optima 8000) and list in Table 1.

2.3. Catalytic performance test

The activity tests of various catalysts were evaluated in a fixed-bed quartz reactor containing 1 g sample. The simulated flue gas contained 500 ppm NO, 500 ppm NH_3, 3% O_2, and N_2 as the balance with a total flow rate of 500 mL/min. The reactor was heated by a temperature-controlled furnace and the measurement was performed at a fixed temperature per 25 °C from 100 to 250 °C. The concentration of outlet NO was monitored by flue gas analyzer (MRU, Germany OPTIMAT7) and the steady-state results were recorded after about 20 min at each objective temperature. The catalytic activity was evaluated by NO conversion according to the following equation:

$$NO\ conversion(\%) = \frac{[NO]_{in} - [NO]_{out}}{[NO]_{in}} \times 100\% \tag{1}$$

where $[NO]_{in}$ was NO inlet concentration (ppm) of the flue gas and $[NO]_{out}$ was NO concentration (ppm) in the outlet.

2.4. Catalyst characterization

Crystal structure of the catalysts was analyzed by the X-ray diffraction (XRD) patterns obtained through a powder diffractometer (Rigaku D/max-2500), using CuKα radiation (λ = 1.5418 Å, 40 kV, 40 mA).

Microscopy images were obtained to analyze the microstructure of the catalysts, using Scanning Electron Micrograph (SEM, VEGAII-LMU/Tescan) at a voltage of 20 kV.

BET surface area, pore volume and average pore diameter were measured by adsorption of N_2 at 77 K, using V-Sorb 2800 BET surface

Table 1
Mass percentage of K and As in the poisoned catalysts.

Samples	K content (wt%)	As content (wt%)
K2.0-Mn-Ce/AC	1.52	–
As-Mn-Ce/AC	–	1.18
K2.0-As-Mn-Ce/AC	1.47	0.98

area analyzer. From the N_2-adsorption isotherm, the specific area of catalyst was obtained based on Brunauer-Emmett-Teller (BET) theory. Micropore volume was calculated by Dubinin–Radushkevich (DR) method. Prior to N_2 adsorption, each sample was degassed in vacuum at 200 °C for 4 h.

Surface atomic state of catalysts was analyzed via X-ray Photoelectron Spectra (XPS). It was measured by Thermo Scientific ESCALAB 250 with Al Kα X-ray (hv = 1486.6 eV) radiation at 150 W. The Binding Energy (BE) was calibrated by using the C1s BE value of 284.6 eV.

Temperature-programmed desorption of NH_3 (NH_3-TPD) was performed with a automatic chemical adsorption apparatus (Autochem II 2920) to study the surface acidity of catalysts. The experiment was carried out with each sample of 100 mg at a total gas flow rate of 50 mL/min. Before temperature-programmed desorption in N_2 (TPD stage) at 10 °C/min from 50 °C to 400 °C, the sample was pretreated in N_2 at 300 °C for 1 h, cooled down to 50 °C and saturated with 10% NH_3/ N_2 for 1 h.

Fourier Transform Infrared Spectroscopy (FT-IR) was recorded with Nicolet 5DXC spectrometer in the range of 4000–400 cm^{-1} to investigate the surface functional groups of catalysts.

3. Results and discussion

3.1. Catalyst activity

The NO conversion of Mn-Ce/AC and Kx-Mn-Ce/AC and As$_2$O$_3$ poisoned catalysts with the variation of reaction temperature ranging from 100 to 250 °C was shown in Fig. 1. From Fig. 1(a), Mn-Ce/AC catalyst showed an excellent SCR performance at low temperature and the highest NO conversion ratio of 94.8% was achieved at 200 °C. A slight activity drop for Mn-Ce/AC catalyst could be observed when the temperature was over 200 °C, while Kx-Mn-Ce/AC catalysts maintain an increasing catalytic activity. Moreover, the addition of KCl caused apparent inhibition effect on catalyst activity. Stronger poisonousness was found with the increasing doping of KCl and NO conversion rate declined to less than 40% at 200 °C for K2.0-Mn-Ce/AC catalyst.

Fig. 1(b) depicted the comparison of with and without As$_2$O$_3$ doping samples over fresh Mn-Ce/AC and K2.0-Mn-Ce/AC catalysts. Compared to Mn-Ce/AC catalyst, NO conversion of poisoning catalyst showed distinct decrease over the whole temperature range. For KCl-doped catalysts, the NO conversion of K2.0-As-Mn-Ce/AC catalyst was much lower than that of K2.0-Mn-Ce/AC catalyst at all temperatures. For As$_2$O$_3$-doping catalysts, the NO conversion curves showed a slight decrease from 125 °C to 150 °C and then increase with the test temperature.

3.2. XRD

Fig. 2 illustrated the XRD patterns of different catalysts. It could be seen that the diffraction peaks belonged to C, CeO$_2$, MnO$_2$ and Mn$_3$O$_4$ were detected on the fresh Mn-Ce/AC catalyst. The intensity of the peaks (near 2θ = 26.73°) related to C for the three poisoned catalysts decreased, indicating that the structure of C in AC had been affected by both KCl and As$_2$O$_3$. No peaks was detected relating to arsenic oxide and KCl, perhaps because the loading content of arsenic oxide and KCl was very low. In addition, they may be amorphous phase on the activated carbon and was dispersed evenly on the surface of catalyst.

3.3. BET and SEM

Fig. 3 illustrated the changes in the micromorphology of different catalysts. It could be found that the surface morphology of catalyst was modified after KCl or As$_2$O$_3$ impregnated. The micrograph of fresh catalyst (Fig. 3(a)) showed apparent porous structure with smooth aperture walls and a few particles attached. From K2.0-Mn-Ce/AC
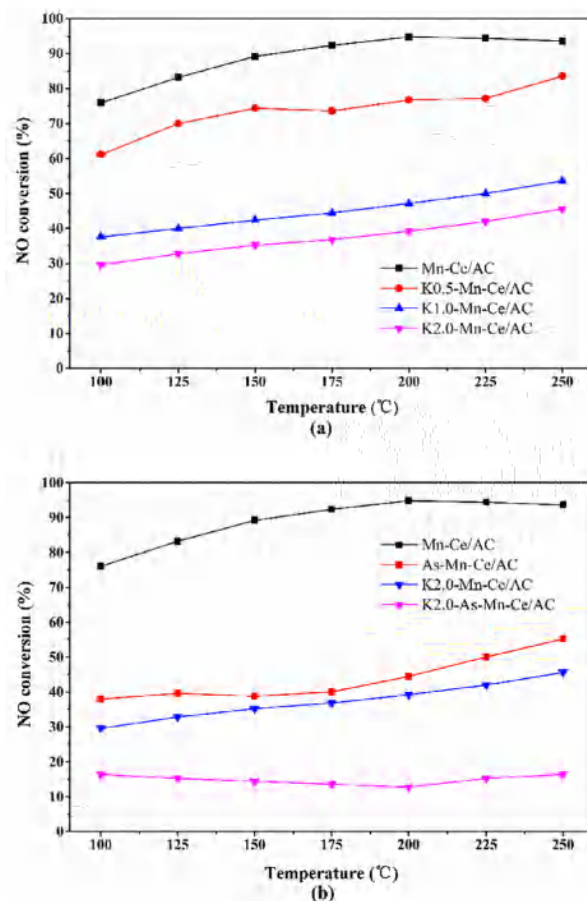
Fig. 1. Variation of NO conversion with reaction temperature 100–250 °C over different (a) KCl, and (b) As$_2$O$_3$ loading catalysts. Reaction conditions: catalyst = 1 g, [NO] = [NH$_3$] = 500 ppm, [O$_2$] = 3%, total flow rate = 500 mL/ min, N$_2$ balance, GHSV = 60000^{-1}.
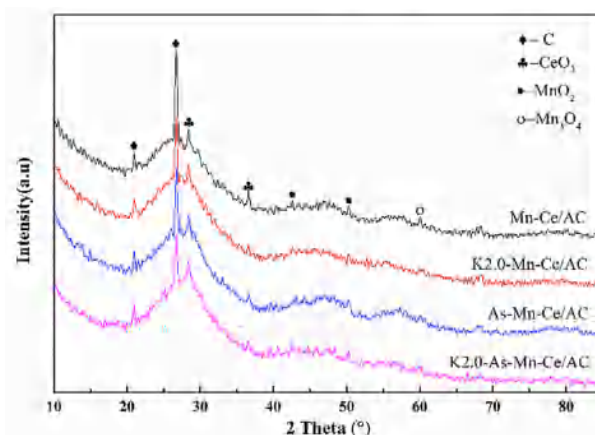
Fig. 2. XRD patterns of different catalysts.

micrograph in Fig. 3(b), the carbon pore was destroyed and the surface of the catalyst became roughened, which made the decrease of BET surface area, total pore volume and average pore diameter (summarized in Table 2). Therefore, the addition of KCl had changed the microstructure of active carbon. Compared with fresh catalyst, the aperture walls of As-Mn-Ce/AC in Fig. 3(c) were thickened. The BET surface area and total pore volume decreased, but no significant change in average pore diameter occurred. These results indicated that the loading of As$_2$O$_3$ caused pore blocked in a way. It could be seen from SEM
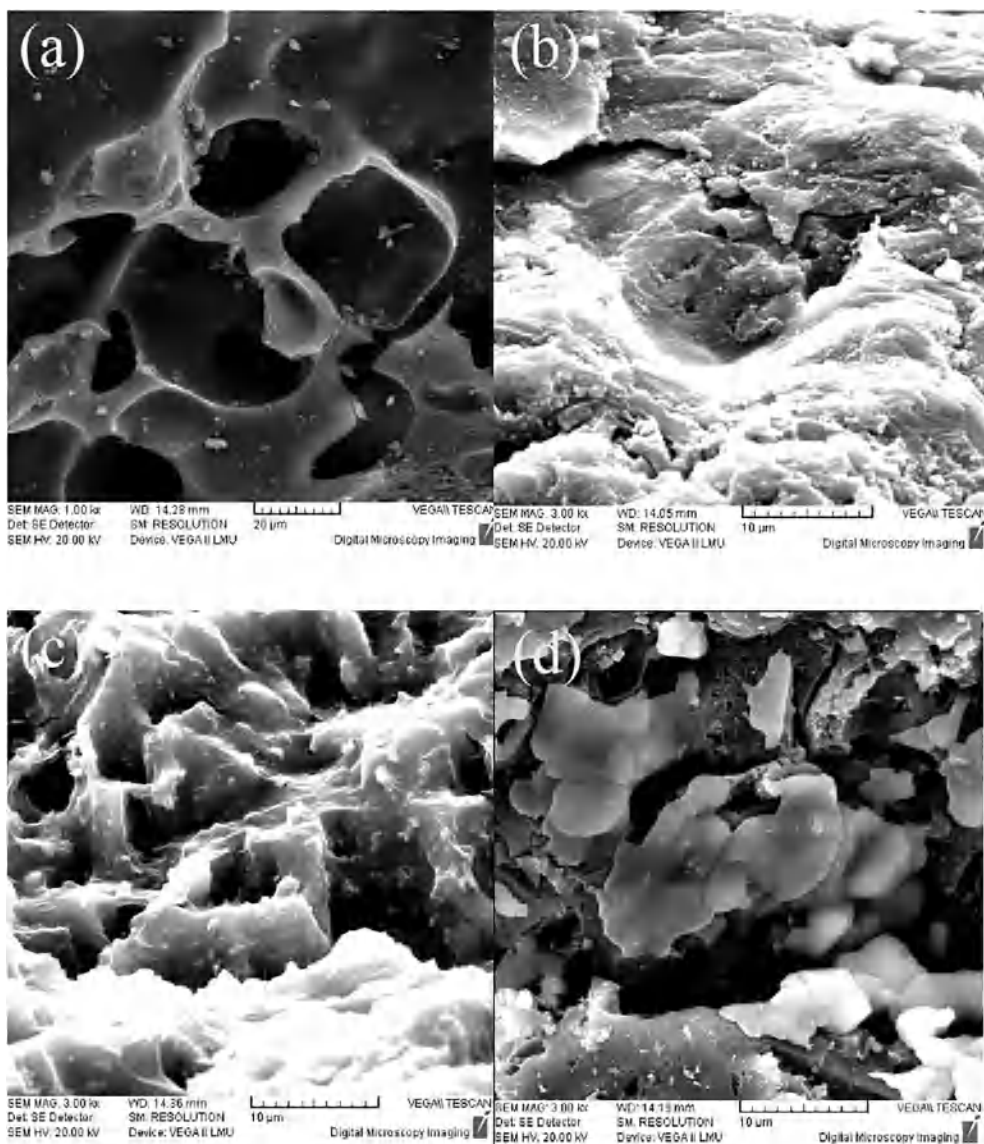
Fig. 3. SEM micrograph of different catalysts: (a) Mn-Ce/AC; (b) K2.0-Mn-Ce/AC; (c) As-Mn-Ce/AC; (d) K2.0-As-Mn-Ce/AC.

Table 2
Physical properties of the catalysts.

Samples	BET surface area (m^2/g)	Total pore volume (cm^3/g)	Average pore diameter (nm)
Mn-Ce/AC	678.107	0.097	3.03
K2.0-Mn-Ce/AC	518.210	0.079	2.78
As-Mn-Ce/AC	564.298	0.086	2.91
K2.0-As-Mn-Ce/AC	414.501	0.074	2.82

micrograph of co-doped KCl and As_2O_3 catalysts (Fig. 3(d)) that a lot of white particles and agglomeration were observed, leading to further reduction of BET surface area and total pore volume.

3.4. XPS

XPS characterization was performed to determine the chemical composition and valence state of elements on the surface of catalysts. Fig. 4 presented the high-resolution XPS spectra at As3d, Ce3d, Mn2p and O1s.

As shown in Fig. 4(a), XPS spectra of As3d were fitted into two peaks centered at 44.6 eV and 45.4 eV. According to the literatures, the peak located at 44.2–45.1 eV can be assigned to As(III) and the binding energy of As(V) is usually 1 eV higher than that of As(III) [19,20]. Therefore, the two peaks could be attributed to As(V) at 45.4 eV and As (III) at 44.6 eV, respectively. The appearance of As(V) species while the original additive was As_2O_3 suggesting that As_2O_3 was oxidized to As_2O_5 in the process of denitrification. The ratio of As(III)/(As(III) + As (V)) was 85.88%, indicating that As(III) was the main As_2O_3 species on the surface of Mn-Ce/AC catalysts. It showed difference with the studies on the arsenic poisoning of VWTi and CeW/Ti catalysts [17,18], which reported that As(V) was the main quantivalence after As_2O_3 adsorption. From the curve of K2.0-As-Mn-Ce/AC, it can be seen that the As(III) increased to 92.82%, which indicated that the addition of KCl inhibited the oxidation of As(III) to As(V).

The Mn2p spectra were presented in Fig. 4(c). There were two main peaks consistent with the spin-orbit doublet of $Mn2p_{1/2}$ and $Mn2p_{3/2}$, locating between 635 and 660 eV. The $Mn2p_{3/2}$ peak can be convoluted to three sub-peaks at 640.48, 641.80 and 644.67 eV, which belong to Mn^{2+}, Mn^{3+} and Mn^{4+}, respectively [21–23]. It meant the co-existence of Mn^{2+}, Mn^{3+} and Mn^{4+} on the surface of catalyst after denitrification. For Mn-Ce/AC catalyst, the ratios of different valence state of MnO_x were 0.25, 0.49 and 0.26 corresponding to Mn^{2+}, Mn^{3+} and
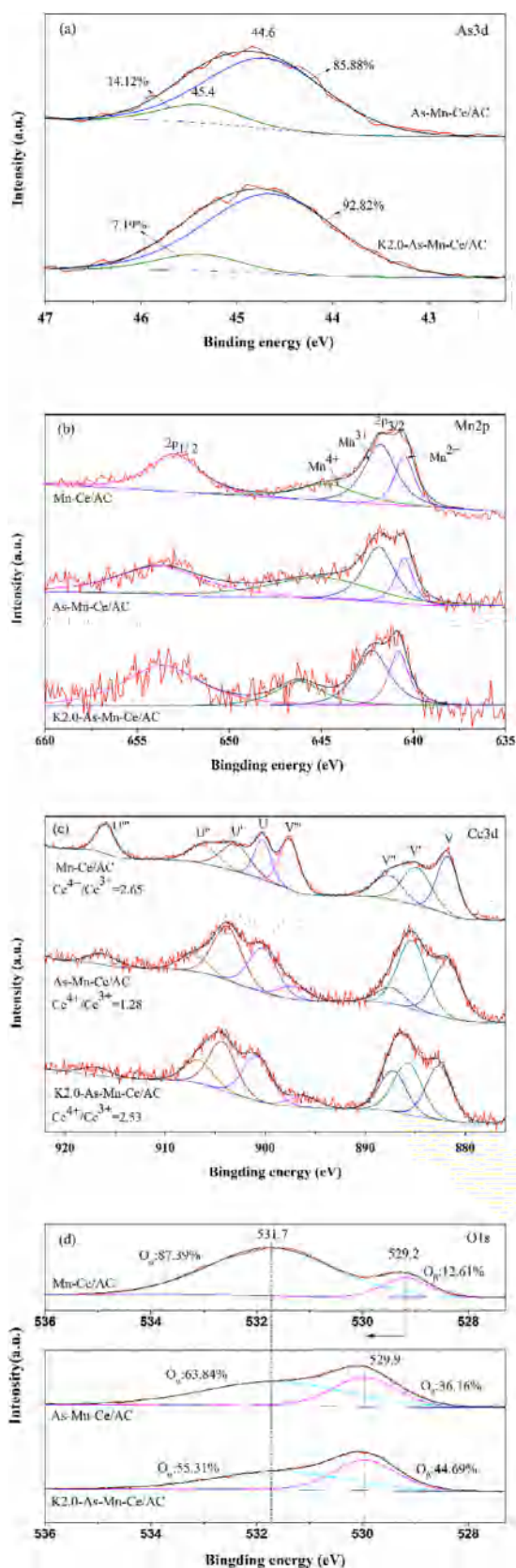
Fig. 4. High-resolution XPS spectra of (a) As3d, (b) Mn2p, (c) Ce3d and (d) O1s.

Mn^{4+}. Whereas the corresponding ratios were 0.17, 0.37, 0.46 for As-Mn-Ce/AC catalyst and 0.26, 0.47, 0.27 for K2.0-As-Mn-Ce/AC catalyst. It indicated that the proportion of Mn^{2+} and Mn^{3+} decreased and

Mn^{4+} proportion increased after As_2O_3 adsorption, which was favor of the reduction of MnO_2. For KCl and As_2O_3 co-doped catalyst, however, the ratio values of different valence state of MnO_x were close to the fresh Mn-Ce/AC catalyst.

Fig. 4(b) showed the XPS spectra of Ce3d. The overlapped peaks denoted as V, V″, V‴, U, U″, U‴ can be attributed to Ce^{4+} species and V′, U′ can be assigned to Ce^{3+} species [16] on the surface of catalysts. The ratio of Ce^{4+}/Ce^{3+} was calculated based on the XPS spectra. The calculated results were 2.65, 1.28 and 2.53 for Mn-Ce/AC, As-Mn-Ce/AC and K2.0-As-Mn-Ce/AC catalyst, respectively. It can be learned that Ce^{4+} was the predominant oxidation state of CeO_x on Mn-Ce/AC catalyst surface. The decrease of Ce^{4+}/Ce^{3+} ratio suggested that the introduction of As_2O_3 caused higher Ce^{3+} concentration. However, the doping of KCl inhibited the increase of Ce^{3+} concentration. The existence of the oxygen vacancies could be accompanied by the presence of Ce^{3+} in the ceria particle and the oxygen vacancies were help for the formation of chemisorbed oxygen on ceria-based catalyst surface [16,24]. Thus, As_2O_3 would increase the amount oxygen vacancies in ceria particle. Zhang et al. [25] researched the influence of K^+ cation on the MnO_x-CeO_2/TiO_2 catalysts and found the oxygen vacancies were occupied by K^+. It can be inferred that the lower Ce^{3+} concentration for K2.0-As-Mn-Ce/AC catalyst compared to single As_2O_3 addition were caused by K^+ occupation.

O1s XPS spectra of different catalysts could be fitted into two sub-peaks relating lattice oxygen (O_β) at 529.2–529.9 eV and chemisorbed oxygen (O_α) at 531.7 eV [9,23,26], such as O^{2-} or O^- belonging to defect-oxide or hydroxyl-like group [27], respectively. As shown in Fig. 4(d), compared with Mn-Ce/AC catalyst, the peak of O_β shifted from 529.2 to 529.9 eV, and the area ratio rose from 12.61% to 36.16% for As-Mn-Ce/AC catalyst and to 44.69% for K2.0-As-Mn-Ce/AC. For As-Mn-Ce/AC catalyst, the portion of O_α decreased, and it may be consumed when As_2O_3 was oxidized to As_2O_5. Compared to As-Mn-Ce/AC catalyst, the ratio of O_α further reduced after KCl doped. Many researches [26,28–30] proposed that chemisorbed oxygen can facilitate SRC performance of catalyst due to its high mobility, so the decreased O_α was responsible for destroying the SCR activity of As-Mn-Ce/AC and K2.0-As-Mn-Ce/AC catalyst.

3.5. NH₃-TPD

NH₃-TPD experiment was carried out to analyze the effect of A_2O_3 and KCl on the surface acidity and ammonia adsorption ability of Mn-Ce/AC catalysts. Fig. 5 showed the NH₃-TPD profile of different catalysts and the total acidity of the catalysts was listed in Table 3. From the profile of all catalysts, one continuous peak in the range of 50–400 °C was observed, indicating that ammonia was adsorbed on the surface of
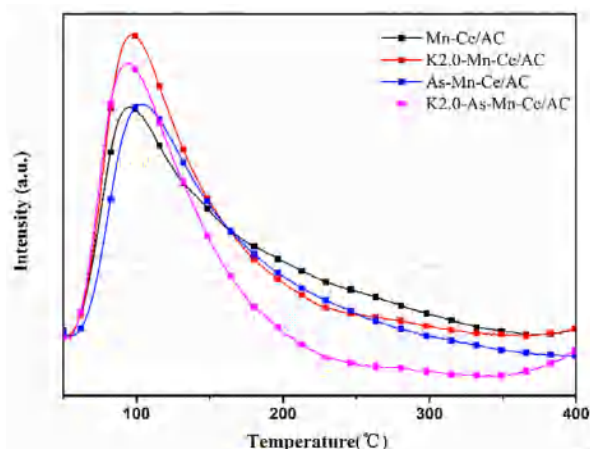
Fig. 5. NH₃-TPD profiles of different catalysts.

Table 3
Surface acidity of fresh and poisoning catalysts.

Samples	Peak center (°C)	Surface acidity (mmol/g)
Mn-Ce/AC	95	0.514
As-Mn-Ce/AC	92	0.372
K2.0-Mn-Ce/AC	97	0.515
K2.0-As-Mn-Ce/AC	93	0.424

these catalysts. This NH_3 desorption peak can be attributed to weak acid sites on Mn-Ce/AC catalyst. As listed Table 3, the doping of As_2O_3 caused a decrease of Mn-Ce/AC surface acidity while KCl had little effect on it, which was also consistent with the NH_3 desorption content of the different catalysts. It indicated that As_2O_3 had an inhibition effect on the NH_3 adsorption performance. But the surface acidity would increase after doping KCl on the As-Mn-Ce/AC catalyst, perhaps because K would occupy the oxygen vacancies on ceria particles and reduced the chemisorbed oxygen on the As-Mn-Ce/AC, which caused the decrease of the oxidization of As_2O_3 and the amount of As_2O_5 covered on the catalyst surface. Thus the decrease of surface acidity should be another reason for decreasing the catalytical activity of As-Mn-Ce/AC and K2.0-As-Mn-Ce/AC catalyst.

3.6. FT-IR

In order to explore the functional-groups situation after doping KCl and As_2O_3, FTIR was carried out. As shown in Fig. 6, the broad band in the range of 3200–3600 cm^{-1} with a maximum near 3447 cm^{-1} were attributed to stretching vibration of −OH in carboxylic, hydroxyl or phenolic groups [31]. However, the band intensity of −OH was weakened obviously for K2.0-Mn-Ce/AC and K2.0-As-Mn-Ce/AC catalysts. Zhang et al. [16] proposed that K^+ cation could bond with –M-OH sites to form -M-O-K complexes. Therefore, it can be inferred that the H atom of −OH groups may be replaced by K, causing −OH groups inactive to adsorb NO and NH_3. The adsorption band at 1634 cm^{-1} corresponded to the stretching of C=O in quinone or carboxylate groups [32] decreased after KCl impregnated. According to the study of Teng et al. [33], adsorption of NO occurs on the C=O part of carboxylic group. Surface oxygen functional groups can improve the dispersion of active phase and form adsorption sites for NH_3 [34]. Hence, the decrease of oxygen functional groups after doping KCl should be a reason for the bad SCR performance of Mn-Ce/AC catalyst.

3.7. Interactions between KCl and As_2O_3 and Mn-Ce/AC catalysts

Based on the experimental results and preceding XPS analysis, the following chain of reactions could represent the synergistic catalytical mechanism of MnO_x and CeO_x on AC in this study:
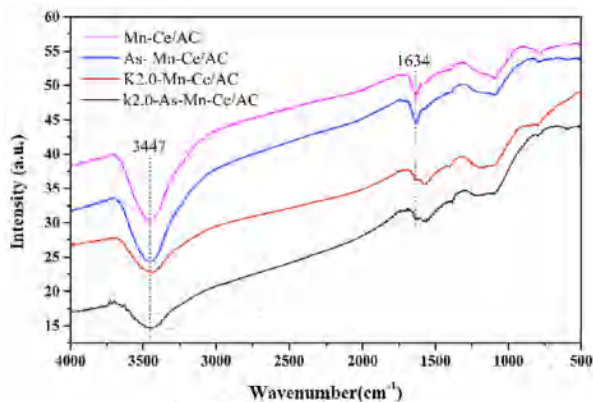
Fig. 6. FT-IR spectra of different catalysts.

$$3MnO_2 \rightarrow Mn_2O_3 + MnO + O_{(a)} \tag{2}$$

$$Mn_2O_3 + MnO + 4CeO_2 \rightarrow 3MnO_2 + 2Ce_2O_3 \tag{3}$$

$$2Ce_2O_3 + O_2 \rightarrow 4CeO_2 \tag{4}$$

$$NH_3(g) \rightarrow NH_3(a) \tag{5}$$

$$NH_3(a) + O(a) \rightarrow NH_2(a) + OH(a) \tag{6}$$

$$NH_2(a) + NO(g) \rightarrow NH_2NO(a) \rightarrow N_2(g) + H_2O \tag{7}$$
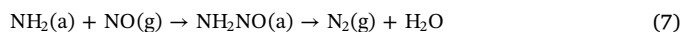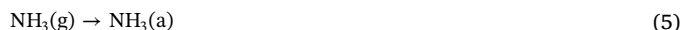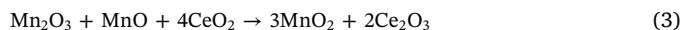
In the process of denitration, MnO_2 was deoxidized to Mn_2O_3 and MnO. The generated oxygen transferred to chemisorbed oxygen ($O_{(a)}$) and it was active in the denitration process NH_3 was firstly adsorbed to the acid sites of MnO_x surface to form coordination NH_3, then the interaction of coordination NH_3 and chemisorbed oxygen of MnO_x surface would react with each other to form −NH_2, Finally, NO and −NH_2 reacted to produce N_2 and H_2O. Meanwhile, the lattice oxygen in CeO_2 was transferred to Mn_2O_3 and MnO, and CeO_2 was reduced to Ce_2O_3. Ce_2O_3 was rapidly oxidized to CeO_2 by O_2 in the flue gas.

When As_2O_3 was added to the catalyst, Mn^{4+} and Ce^{3+} increased while Mn^{3+}, Mn^{2+} and Ce^{4+} decreased, which was conducive to enhance catalyst activity. But from the results of denitration experiment, deactivation of catalyst was observed obviously. It can be concluded that As_2O_3 was oxidized to As_2O_5 maybe by means of consuming the generated oxygen during the reduction of MnO_2 (Eq. (2)), which was not beneficial to form −NH_2 (Eq. (6)).

According to FT-IR results, KCl caused a marked decrease for the intensity of −OH and C=O band. Based on the analysis of FT-IR and the results of experiments, interaction probably occurred between KCl and oxygen functional groups on the surface of catalyst. The reaction might be described as follows:

$$R−OH + KCl \rightarrow R−O− K+ HCl \tag{8}$$

$$HCl + R'− C= O \rightarrow R'−C(Cl)−O−H \tag{9}$$

$$R'−C(Cl)−O− H+ KCl \rightarrow R'−C(Cl)−O− K+ HCl \tag{10}$$
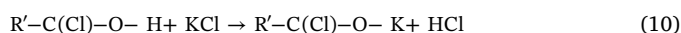
In the reactions above, R−OH and R'−C=O represented −OH groups and C=O groups on the surface of catalyst, respectively. The interaction was schematically shown in Fig. 7. First, KCl interacted with R-OH to form R-O-K complex and H replaced by K combined with Cl^- to form HCl (Eq. (8)). Then the obtained HCl reacted with R−C=O to form R−C (Cl)−O−H (Eq. (9)). The generated R−C(Cl)−O−H proceeded to react with KCl, then the complex of R−C(Cl)−O−K was formed finally (Eq. (10)). Subsequently, the reaction cycle was built up.

3.8. KCl and As_2O_3 poisoning mechanism model of Mn-Ce/AC catalysts

Based on above analysis, the synergetic poisoning mechanism model of KCl and As_2O_3 on Mn-Ce/AC catalyst can be reasonably deduced and was given in Fig. 8. From the figure, the adsorbed As_2O_3 was oxidized to As_2O_5 by chemisorbed oxygen on MnO_x surface. The reaction could be
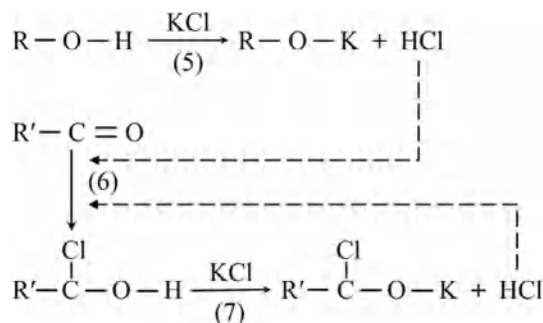
Fig. 7. Schematic diagram of interaction between KCl and oxygen functional groups on Mn-Ce/AC SCR catalysts.
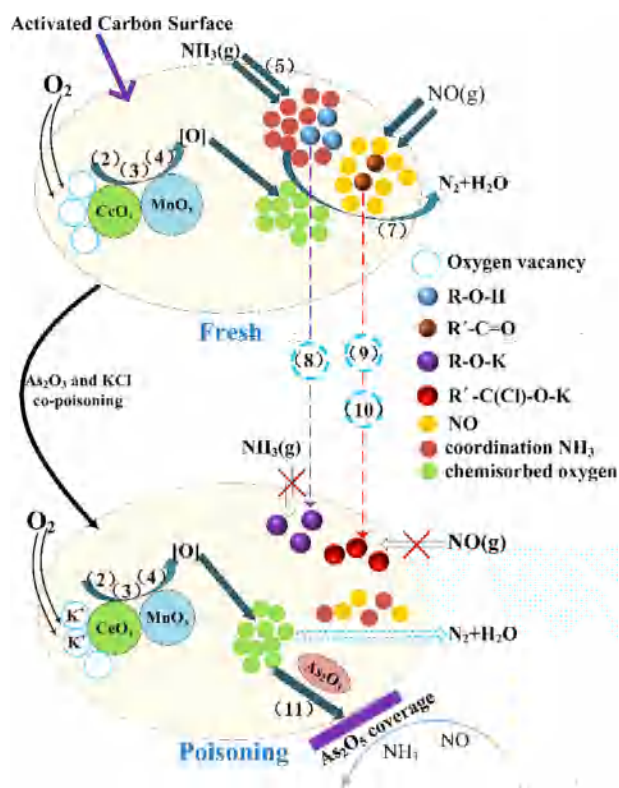
Fig. 8. Schematic diagram of synergy effects of As₂O₃ and KCl on Mn-Ce/AC catalyst.

described as follows:

$$As_2O_3 + 2O_{(a)} \rightarrow As_2O_5 \tag{11}$$

In the SCR process of NH₃ with NO, the lattice oxygen of MnO₂ was transferred to O$_{(a)}$ (Eq. (2)) to participate in the denitration reaction. The O$_{(a)}$ on MnO$_x$ surface was consumed in the oxidation process of As₂O₃ (Eq. (11)). Therefore, the oxygen transferred from Mn-Ce/AC catalyst to the denitration process was reduced. Besides, K would occupy the oxygen vacancies on ceria particles, which weakened the redox cycle of Ce^{3+} ↔ Ce^{4+} (Eq. (4)). And the weakened redox cycle of Ce^{3+} ↔ Ce^{4+} would inhibited the reactions (Eqs. (2) and (3)) between MnO$_x$ and CeO$_x$ and finally reduced the chemisorbed oxygen. All of these could cause the decrease of −NH₂ formed by Eq. (6).

The produced solid As₂O₅ formed some coverage on the catalyst surface, causing the pore structure of AC blocked and part active sites on catalysts covered. The surface acidity of catalysts was also declined. Ultimately, the adsorption and activation of NH₃ and NO for Mn-Ce/AC catalyst were decreased. Besides, the presence of surface functional groups can form adsorption sites and increase NH₃ and NO sorption capacity. However, the interaction between KCl and oxygen functional groups of AC (Eqs. (8)–(10)) resulted in the decrease of −OH groups and C=O groups on the surface of Mn-Ce/AC catalyst (From Fig. 6). The decrease of adsorption capacity of NH₃ and NO was not beneficial for the reaction rate of Eqs. (6) and (7), which could cause the decrease of activity of the catalyst.

In addition, the addition of As₂O₃ and KCl caused the decrease of the total surface area and pore volume of AC and pore blocked in a way (From Fig. 3 and Table 2). The decrease of the peaks related to C for the three poisoned catalysts (from Fig. 2) indicated that the structure of C in AC had been affected by both KCl and As₂O₃. All these were harmful for the process of denitration.

Therefore, the change of the AC structure and the reduction of chemisorbed oxygen, the adsorption and the activation of NO and NH₃ caused Mn-Ce/AC catalysts lost activity in the SCR process of NH₃ with NO.

4. Conclusions

Both KCl and As₂O₃ performed serious deactivation over Mn-Ce/AC catalysts for the SCR of NO with NH₃, and the poisoning effect increased with the increase of KCl doping amount. The characteristics of fresh, KCl-, As₂O₃- and common poisoning catalysts were characterized by XRD, SEM, BET, XPS, NH₃-TPD and FT-IR. The results showed that KCl destroyed the pore structure of AC, and decreased the BET surface area, total pore volume and average pore diameter. According to the analysis of XPS, oxygen vacancies in ceria particle and chemisorbed oxygen on Mn-Ce/AC catalyst were decreased after KCl doped. Form FT-IR results, functional groups was affected evidently by KCl, which caused the decrease of NH₃ and NO adsorption. From the results of SEM and XPS, As₂O₃ was oxidized to As₂O₅ by chemisorbed oxygen. The layer of As₂O₅ was covered on the hole wall of Mn-Ce/AC catalyst and reduced the BET surface area and total pore volume, leading to the decrease of NO and NH₃ adsorption. Besides, As₂O₃ could increase the number of oxygen vacancies and reduce the surface acidity of Mn-Ce/AC catalyst. No obvious changes were observed in the crystalline phase for MnO$_x$ or CeO$_x$ on all samples. In this way, the change of the AC structure and the reduction of surface chemisorbed oxygen, NH₃ and NO adsorption, resulted from the combined effect of KCl and As₂O₃, was responsible for the deactivation of Mn-Ce/AC catalyst. Based on the experimental results and theoretical analysis, the probable KCl-poisoning mechanism and the synergy poisoning effect model of KCl and As₂O₃ on Mn-Ce/AC catalyst was proposed schematically.

References

[1] R.T. Guo, W.G. Pan, J.X. Ren, X.B. Zhang, Q. Jin, Absorption of NO from simulated flue gas by using NaClO₂/(NH₄)₂CO₃ solutions in a stirred tank reactor, Korean J. Chem. Eng. 30 (2013) 101–104.
[2] R.T. Guo, W.L. Zhen, W.G. Pan, Y. Zhou, J.N. Hong, H.J. Xu, Q. Jin, C.G. Ding, S.Y. Guo, Effect of Cu doping on the SCR activity of CeO₂ catalyst prepared by citric acid method, J. Ind. Eng. Chem. 20 (2014) 1577–1580.
[3] X. Gao, Y. Jiang, Y. Zhong, Z. Luo, K. Cen, The activity and characterization of CeO₂-TiO₂ catalysts prepared by the sol-gel method for selective catalytic reduction of NO with NH₃, J. Hazard Mater. 174 (2010) 734.
[4] R.T. Guo, Y. Zhou, W.G. Pan, J.N. Hong, W.L. Zhen, Q. Jin, C.G. Ding, S.Y. Guo, Effect of preparation methods on the performance of CeO₂/Al₂O₃ catalysts for selective catalytic reduction of NO with NH₃, J. Ind. Eng. Chem. 19 (2013) 2022–2025.
[5] B. Thirupathi, P.G. Smirniotis, Nickel-doped Mn/TiO₂ as an efficient catalyst for the low-temperature SCR of NO with NH₃: catalytic evaluation and characterizations, J. Catal. 288 (2012) 74–83.
[6] X.P. Zhang, B.X. Shen, Selective catalytic reduction of NO with NH₃ over Mn-based catalysts at low temperature, J. Fuel Chem. Technol. 41 (2013) 123–128.
[7] C. Fang, D. Zhang, S. Cai, L. Zhang, L. Huang, H. Li, P. Maitarad, L. Shi, R. Gao, J. Zhang, Low-temperature selective catalytic reduction of NO with NH₃ over nanoflaky MnO$_x$ on carbon nanotubes in situ prepared via a chemical bath deposition route, Nanoscale 5 (2013) 9199.
[8] H. Huang, W. Shan, S. Yang, J. Zhang, Novel approach for a cerium-based highly-efficient catalyst with excellent NH₃-SCR performance, Catal. Sci. Technol. 4 (2014) 3611–3614.
[9] L. Zhou, C. Li, L. Zhao, G. Zeng, L. Gao, Y. Wang, M.E. Yu, The poisoning effect of PbO on Mn-Ce/TiO₂ catalyst for selective catalytic reduction of NO with NH₃ at low temperature, Appl. Surf. Sci. 389 (2016) 532–539.
[10] X. Wang, Y. Zheng, J. Lin, Highly dispersed Mn–Ce mixed oxides supported on carbon nanotubes for low-temperature NO reduction with NH₃, Catal. Commun. 37 (2013) 96–99.
[11] X. You, Z. Sheng, D. Yu, L. Yang, X. Xiao, S. Wang, Influence of Mn/Ce ratio on the physicochemical properties and catalytic performance of graphene supported MnOx-CeO₂ oxides for NH₃-SCR at low temperature, Appl. Surf. Sci. 423 (2017).
[12] A. Oberlin, Carbonization and graphitization, Carbon 22 (1984) 521–541.
[13] J.H. Zhou, Z.J. Sui, J. Zhu, P. Li, D. Chen, Y.C. Dai, W.K. Yuan, Characterization of surface oxygen complexes on carbon nanofibers by TPD, XPS and FT-IR, Carbon 45 (2007) 785–796.
[14] A. Boyano, M.E. Gálvez, R. Moliner, M.J. Lázaro, Carbon-based catalytic briquettes for the reduction of NO: effect of H₂SO₄ and HNO₃ carbon support treatment, Fuel 87 (2008) 2058–2068.
[15] Z. Zhu, Z. Liu, S. Liu, H. Niu, A novel carbon-supported vanadium oxide catalyst for NO reduction with NH₃ at low temperatures, Appl. Catal. B-Environ. 23 (1999) 229–233.
[16] L. Zhang, S. Cui, H. Guo, X. Ma, X. Luo, The influence of K⁺ cation on the MnO$_x$

NO.

-CeO$_2$/TiO$_2$ catalysts for selective catalytic reduction of NO$_x$ with NH$_3$ at low temperature, J. Mol. Catal. A-Chem. 390 (2014) 14–21.

[17] M. Kong, Q. Liu, X. Wang, S. Ren, J. Yang, D. Zhao, W. Xi, L. Yao, Performance impact and poisoning mechanism of arsenic over commercial V$_2$O$_5$–WO$_3$/TiO$_2$ SCR catalyst, Catal. Commun. 72 (2015) 121–126.

[18] L. Xiang, J. Li, P. Yue, H. Chang, Z. Tao, Z. Shen, W. Si, J. Hao, Mechanism of arsenic poisoning on SCR catalyst of CeW/Ti and its novel efficient regeneration method with hydrogen, Appl. Catal. B-Environ. 184 (2016) 246–257.

[19] C.D. Wagner, Handbook of X-ray Photoelectron Spectroscopy, Perkin-Elmer, 1979.

[20] C.A. Martinson, K.J. Reddy, Adsorption of arsenic(III) and arsenic(V) by cupric oxide nanoparticles, J. Colloid Interf. Sci. 336 (2009) 406–411.

[21] B. Zhao, R. Ran, X. Guo, L. Cao, T. Xu, Z. Chen, X. Wu, Z. Si, D. Weng, Nb-modified Mn/Ce/Ti catalyst for the selective catalytic reduction of NO with NH$_3$ at low temperature, Appl. Catal. A-Gen. 545 (2017) 64–71.

[22] H.W. Nesbitt, D. Banerjee, Interpretation of XPS Mn(2p) spectra of Mn oxyhydr-oxides and constraints on the mechanism of MnO$_2$ precipitation, Am. Mineral. 83 (2015) 305–315.

[23] N.J. Fang, J.X. Guo, S. Shu, J.J. Li, Y.H. Chu, Influence of textures, oxygen-con-taining functional groups and metal species on SO$_2$ and NO removal over Ce-Mn/NAC, Fuel 202 (2017) 328–337.

[24] P. Dutta, A.S. Pal, M.S. Seehra, Y. Shi, E.M.E. And, R.D. Ernst, Concentration of Ce^{3+} and oxygen vacancies in cerium oxide nanoparticles, Chem. Mater. 18 (2006) 5144–5146.

[25] H. Wang, X. Chen, S. Gao, Z. Wu, Y. Liu, X. Weng, Deactivation mechanism of Ce/TiO$_2$ selective catalytic reduction catalysts by the loading of sodium and calcium salts, Catal. Sci. Technol. 3 (2013) 715–722.

[26] R.T. Guo, C.Z. Lu, W.G. Pan, W.L. Zhen, Q.S. Wang, Q.L. Chen, H.L. Ding, N.Z. Yang, A comparative study of the poisoning effect of Zn and Pb on Ce/TiO$_2$ catalyst for low temperature selective catalytic reduction of NO with NH$_3$, Catal. Commun. 59 (2015) 136–139.

[27] H. Park, D.H. Yeom, J. Kim, J.K. Lee, MnO/C nanocomposite prepared by one-pot hydrothermal reaction for high performance lithium-ion battery anodes, Korean J. Chem. Eng. 32 (2015) 178–183.

[28] L. Chen, J. Li, M. Ge, The poisoning effect of alkali metals doping over nano V$_2$O$_5$–WO$_3$/TiO$_2$ catalysts on selective catalytic reduction of NO$_x$ by NH$_3$, Chem. Eng. J. 170 (2011) 531–537.

[29] K.J. Lee, P.A. Kumar, M.S. Maqbool, K.N. Rao, K.H. Song, H.P. Ha, Ceria added Sb-V$_2$O$_5$/TiO$_2$ catalysts for low temperature NH$_3$ SCR: physico-chemical properties and catalytic activity, Appl. Catal. B-Environ. 142 (2013) 705–717.

[30] R.T. Guo, Q.S. Wang, W.G. Pan, W.L. Zhen, Q.L. Chen, H.L. Ding, N.Z. Yang, C.Z. Lu, The poisoning effect of Na and K on Mn/TiO$_2$ catalyst for selective catalytic re-duction of NO with NH$_3$: a comparative study, Appl. Surf. Sci. 317 (2014) 111–116.

[31] S. Biniak, G. Szymański, J. Siedlewski, A. Świątkowski, The characterization of activated carbons with oxygen and nitrogen surface groups, Carbon 35 (1997) 1799–1810.

[32] S. Hermans, C. Diverchy, O. Demoulin, V. Dubois, E.M. Gaigneaux, M. Devillers, Nanostructured Pd/C catalysts prepared by grafting of model carboxylate com-plexes onto functionalized carbon, J. Catal. 243 (2006) 239–251.

[33] H. Teng, Y.T. Tu, Y.C. Lai, C.C. Lin, Reduction of NO with NH$_3$ over carbon cata-lysts: the effects of treating carbon with H$_2$SO$_4$ and HNO$_3$, Carbon 39 (2001) 575–582.

[34] L. Zhu, B. Huang, W. Wang, Z. Wei, D. Ye, Low-temperature SCR of NO with NH$_3$ over CeO$_2$ supported on modified activated carbon fibers, Catal. Commun. 12 (2011) 394–398.